Temporal criticality

José Moran, Matthijs Romeijnders, Frank P. Pijpers, Utz Weitzel, Debabrata Panja and Jean-Philippe Bouchaud

27 Sept 2023

Temporal criticality

José Moran
Institute for New Economic Thinking at the Oxford Martin School,
University of Oxford, Oxford, United Kingdom
Complexity Science Hub, Vienna, Austria

Matthijs Romeijnders
Department of Information and Computing Sciences, Utrecht University, The Netherlands

Pierre Le Doussal
Laboratoire de Physique de l'École Normale Supérieure, ENS,
Université PSL, CNRS, Sorbonne Université, Université de Paris, France

Frank P. Pijpers
Statistics Netherlands
and Korteweg-de Vries Institute for Mathematics,
University of Amsterdam, The Netherlands

Utz Weitzel
School of Business and Economics, Vrije Universiteit Amsterdam, Amsterdam, The Netherlands
Tinbergen Institute, Amsterdam, The Netherlands
Nijmegen School of Management, Radboud University, Nijmegen, The Netherlands

Debabrata Panja
Department of Information and Computing Sciences, Utrecht University, The Netherlands
Centre for Complex Systems Studies, Utrecht University, The Netherlands[*]

Jean-Philippe Bouchaud
Capital Fund Management, Paris, France
X-CFM Chair of EconophysiX,
Ecole polytechnique, Palaiseau, France
(Dated: September 27, 2023)

In complex systems, external parameters often determine the phase in which the system operates, i.e., its macroscopic behavior. For nearly a century, statistical physics has extensively studied systems' transitions across phases, (universal) critical exponents, and related dynamical properties. Here we consider the functionality of systems, notably operations in socio-technical ones, production in economic ones and possibly information-processing in biological ones, where timing is of crucial importance. We introduce a stylized model on temporal networks with the magnitude of delay-mitigating buffers as the control parameter. The model exhibits *temporal criticality*, a novel form of critical behavior *in time*. We characterize fluctuations near criticality, commonly referred to as "avalanches", and identify the corresponding critical exponents. We show that real-world temporal networks, too, exhibit temporal criticality. We also explore potential connections with the Mode-Coupling Theory of glasses and the directed polymer problem.

I. INTRODUCTION

The value of *timeliness* — goods, services, or people being in the right place at the right time — can hardly be overstated. For example, the value of a train ride or food greatly depreciates in the absence of timely provision. From the perspective of socio-technical systems (STSs), where technological and human elements interact to provide functional support to our societies, the user-centric examples above translate into the timely availability of crew, infrastructure and material in transport

systems, and into the timely production, processing and distribution in food systems to match demand in a timely manner. The concept of timeliness has been ubiquitously and integrally adopted as a quality standard across STSs, reaching beyond transport and food into energy systems (where timeliness prevents blackouts), financial markets (which need liquidity on time), and all other systems of exchange and production that rely on the timely supply of raw materials, goods, services, and offers to trade.

There exist a variety of incentives for STS operators, often reinforced by competitive pressures, to increase cost- and time-efficiencies in order to achieve superior operational results [1]. For example, train operators may have the goal to maximize the number of passengers to

be transported by the network, i.e., to fit trains into ever tighter schedules. This can be achieved by reducing the *temporal buffer* that allows the system to absorb possible delays. Operators could, for example, shorten stopping times of trains in stations or reduce the amount of replacement crews on standby. In the extreme (hypothetical) case of zero temporal buffers in the whole system, the delay of an arriving train is directly copied to the departing train: clearly, any delay, however small, will reverberate through the entire system [2, 3]. The purpose of this paper is to demonstrate, in terms of a stylized model, that efficiency incentives, in combination with maintaining timeliness as a quality standard for system operations, give rise to the phenomenon of *temporal criticality*, a critical phenomenon, but in the temporal dimension.

Our model can easily be extended to other types of STSs, including the propagation of supply fluctuations in production networks, where firms reduce costs by keeping the inventory of production inputs at a minimal level [4, 5]. Any delay in such a "just in time" supply chain can easily propagate down the production network [6], with major disruptions, as exemplified by the Suez canal obstruction by a single container ship in 2021 [7]. In fact, inventories can help to significantly mitigate the economic effects of natural disasters [8], but even in less extreme conditions, low levels of inventories or of supplier redundancy can cause strong output fluctuations of firm networks (see e.g. [9, 10] and references cited therein).[1]

More generally, our model can characterize any network of interacting elements operating over time, and where the output of one stage becomes the input for the next. The flows of these inputs and outputs in these *temporal networks* can be disrupted and delayed, with effects cascading down to other components. The key aspect of our model is that the components of the system can integrate temporal buffers that allow them to mitigate these disruptions.

The aim of the present paper is to propose a minimal, stylized model that reveals the existence of a temporal critical point in these systems as the size of the mitigating buffers is reduced. More precisely, above a certain critical buffer size, delays cannot propagate and system-wide crises are avoided. On the contrary, when temporal margins are not wide enough, delays accumulate without bounds, leading to systemic failures.

Our model is closely related to the so-called "Bounded Kardar-Parisi-Zhang" (B-KPZ) equation [11, 12], that describes the motion of a driven interface in the presence of a hard wall preventing the interface to visit the

lower half space. Depending on the driving field, the interface is either localized around the hard wall, or undergoes an unbinding transition and escapes to infinity. Our model precisely describes such unbinding transition in the mean-field limit, where we find unexpected (and little understood at this stage) analogies with the Mode Coupling Theory of the glass transition [13].

The structure of this paper is as follows. We describe and analyze the stylized models, and identify the critical transitions in Sec. II. In Sec. III we characterize the critical scalings in terms of diverging temporal correlations, avalanche durations and sizes, and variograms of fluctuation statistics. In Sec. IV we demonstrate the existence of criticality also in real-world temporal networks. We then conclude the paper by a discussion in Sec. V. Calculations supporting the results are in Supplementary Information (SI) A through E.

II. TEMPORAL CRITICALITY

Although initially formulated to investigate the propagation of delays in rail networks [2], our model is flexible enough to be applied to a wide array of systems. It is in fact a representation of any form of planning schedule depicting temporal ordering of different events that (have to) depend on each other, and therefore, best formulated in terms of *temporal networks* [14, 15]. We describe the mathematical structure of our model below.

A. Temporal networks

In general terms, the delay $\tau_i(t)$ suffered by a component $i \in [\![1, N]\!]$ of the system at the t-th step of schedule, $t \in \mathbb{N}$, can be written as [2]

$$\tau_i(t) = \max_j \left[\sum_{t'=0}^{t-1} A_{ij}(t, t') \tau_j(t') - B_{ij}(t) \right]^+ + \varepsilon_i(t), \ (1)$$

where $\mathbf{A}(t, t')$ is the binary *temporal adjacency matrix* of the network, indicating whether a delay of component j at time t' has an effect on the delay of component i at time t, $B_{ij}(t)$ indicates the buffer that component i has over component j at time t, and $\varepsilon_i(t)$ is a random process encoding fluctuations affecting component i at time t, with $[x]^+ := \max(0, x)$. Figure 1(a) provides a succinct representation of this structure. For firm input-output production systems the first term on the rhs can be interpreted in terms of a firm i whose production is affected at time t because of delays on shipments from its clients j that were sent out at an earlier time t'. Further, B_{ij} is the *temporal buffer*: as explained in the introduction, it is a quantity of relevance in its own right for transport systems, and for firm input-output networks it is related to the amount of time firm i can continue producing without being affected by a loss of inputs from firm j.

---

[1] Other fields of applications of our model may be distributed computing systems where the result of some computation must arrive before another computation can start. Outside of STSs, our model of temporal networks may be relevant for the understanding of neural processes in clinical and behavioral neuroscience and for other biological contexts.
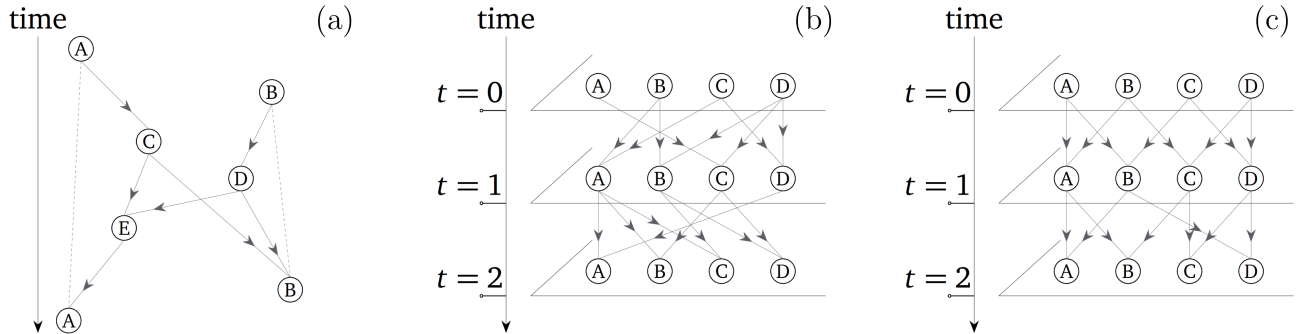
FIG. 1. Schematics of our model in terms of temporal networks. (a) How the (time-ordered) dependencies — shown by arrows — among the system components (number of components $N = 5$) in a real-world situation may play out [Eq. (1)]. A mean-field (MF) (b) and a synthetic temporal network (STN) (c) representation respectively of our stylized model (number of components $N = 4$) in discretized time steps [Eq. (2)]. For both the MF and the STN cases, the number of arrows K entering every system component is constant (e.g., $K = 2$); for the latter case the number of arrows leaving every system component is also K.

Equation (1) is very general, and should in principle be accompanied by equations that specify the dynamics of the buffers B_{ij} (for example as the inventories of firms get depleted) and of the adjacency matrix $\mathbf{A}$ (encoding firms that switch suppliers or transport vehicles and personnel that are rerouted, for example; that is to say that, in reality, a delay at time t can impact the topology of the temporal network). Here we propose a much simpler framework.

The first steps in simplifying Eq. (1) are as follows: (a) assume that the dynamical evolution is "Markovian"[2], in the sense that the delay at layer t only depends on events at $t-1$, so that $A_{ij}(t,t') \equiv A_{ij}(t-1)\delta_{t',t-1}$, (b) we take $B_{ij}(t) = B$ to be constant and identical across all pairs of components. Together these lead to the following stylized equation

$$\tau_i(t) = \left[\max_j \left[A_{ij}(t-1)\tau_j(t-1)\right] - B\right]^+ + \varepsilon_i(t). \quad (2)$$

The adjacency matrix $A_{ij}(t)$ also remains to be defined. We work in the thermodynamic limit $N \to \infty$ and introduce two variants: (1) *mean-field* (MF), where a system component can be delayed by K randomly chosen and statistically independent components that are redrawn at every time-step t, meaning $\sum_j A_{ij}(t-1) = K$ [Fig. 1(b)], and (2) *synthetic temporal network* (STN) that imposes further constraints, such as $\sum_j A_{ij}(t-1) = \sum_j A_{ji}(t-1) = K$ [Fig. 1(c)].

Finally, the statistics of the noise ε_i need to be specified. In line with the Markovian assumption above, we take them to be iid (independent both in the component

i and time-step t) realizations of the same random variable. Only the MF case with exponentially-distributed noise allows us to find an analytical solution.

For the sake of brevity, we keep the example of the input-output network and use 'firm' to mean 'system component' throughout the rest of the paper.

B. Criticality

An analytical solution of Eq. (2) in the mean-field case can be provided if we take ε to be an exponentially distributed random variable, with density $P(\varepsilon) = \mathbf{1}_{\varepsilon>0}\nu \exp(-\nu\varepsilon)$. Without any loss of generality we take $\nu = 1$, choosing ν^{-1} as the unit for the buffer B and the delays τ.

We analyze $\psi_t(\tau)$, the distribution of the delays at time t in the following manner. Having defined $\Psi_t(\tau) = \int_\tau^\infty du\ \psi_t(u)$, the complementary cumulative density function of the delays, and $Q_t(\tau) = K\psi_t(\tau)[1 - \Psi_t(\tau)]^{K-1}$, the probability density of the maximum of K randomly chosen delays, Eq. (2) becomes (SI A)

$$\psi_t(\tau) = \int_0^\tau d\varepsilon\ P(\varepsilon)\ Q_{t-1}(\tau + B - \varepsilon) + P(\tau)\int_0^B du\ Q_{t-1}(u),$$
(3)

which is readily obtained by considering splitting Eq. (2) into two cases: the first contribution corresponds to the maximal delay at the previous time-step being equal to $\tau+B-\varepsilon$ (i.e., larger than B from which the buffer absorbs B amount of delay), while the second one comes from the case when the maximum of the K randomly chosen delays is smaller than B. With $P(\varepsilon) = \mathbf{1}_{\varepsilon>0}\exp(-\varepsilon)$, Eq. (3)

_____
[2] In the most general case, an event at time t can be delayed by any event at a time $t' < t$. We restrict ourselves to the case where events can only affect events in the next time-step.
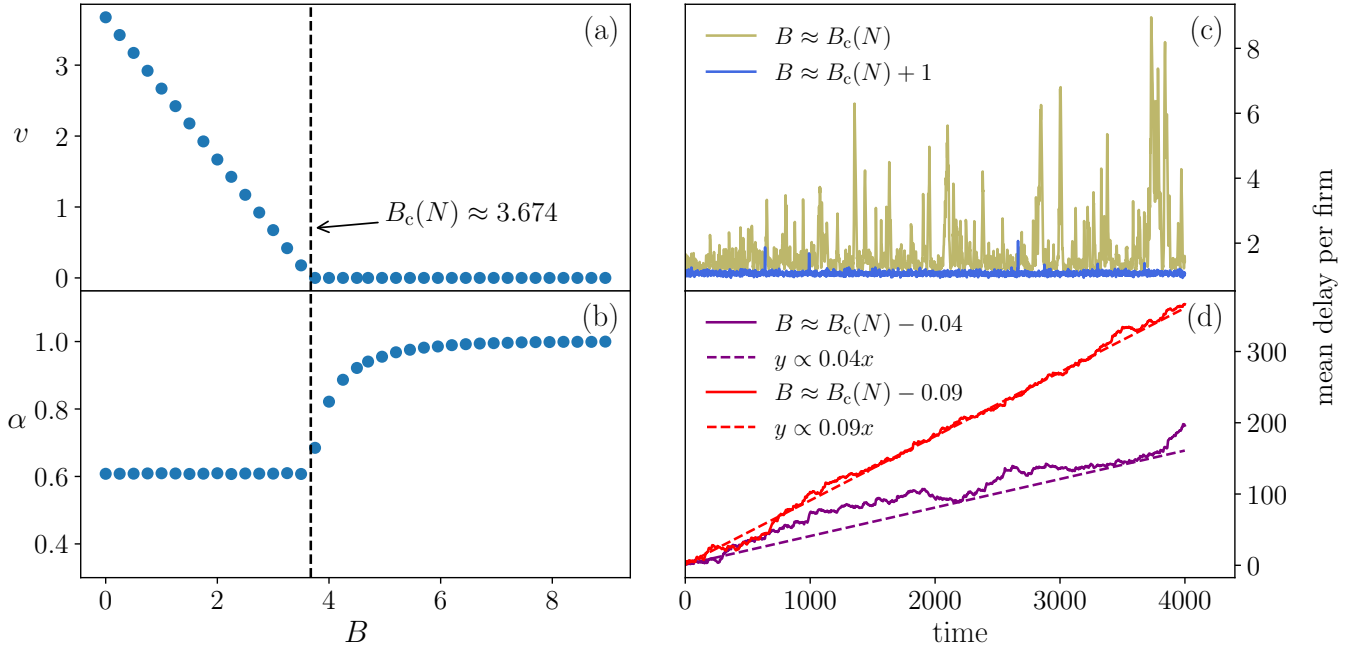
FIG. 2. (a-b) Temporal criticality in the stylized model obtained from direct simulations of Eq. (2) with exponentially distributed noise for $N = 10,000$ and $K = 5$: both the order parameter v and the exponent α for the exponentially decaying tail of the delay distribution function $\psi(\tau)$. The critical value of the temporal buffer $B_c(N)$ is found to be ≈ 3.674. (c-d) typical behavior of the mean delay per firm $\sum_i \tau_i/N$, as a function of the temporal depth t: when the buffer is smaller than the critical buffer $B_c(N)$ the mean delay per firm keeps accumulating without bound; in contrast, avalanches of all sizes appear spontaneously in the mean delay per firm when the buffer is smaller than $B_c(N)$, with no relation to the amplitude of the initial values of the noise term. The dashed lines show a fit through the data over a long period of time.

can be simplified to derive (SI A)

$$\Psi_t''(\tau) + \Psi_t'(\tau) = K[1 - \Psi_{t-1}(\tau + B)]^{K-1} \Psi_{t-1}'(\tau + B). \tag{4}$$

In the limit of large temporal depth $t \to \infty$, we surmise (and check *a posteriori*) that the distribution of τ must have an exponential tail, leading to two different cases (SI B). In the first case, $\psi_t(\tau)$ and $\Psi_t(\tau)$ reach a stationary state asymptotically, with exponential tails $\propto \exp(-\alpha\tau)$ for some (inverse-time) parameter α.[3] This type of solution exists only when B is larger than a critical value B_c^*, given by the condition (SI B)

$$B_c^* \exp(1 - B_c^*) = \frac{1}{K}, \tag{5}$$

with an analytical solution $B_c^* = -W_{-1}(-1/(eK))$, with $W_{-1}(x)$ the branch of the Lambert function with values

---

[3] This is a natural assumption, because the exponential distribution is in the Gumbel maximum universality class, and so the maximum of a large number of exponential random variables has a distribution with an exponential tail. Similarly, when $B \to \infty$ one simply has $\tau_i(t) = \varepsilon_i(t)$, and the delays are exponentially distributed with $\alpha = 1$.

in $[-1, -\infty[$ for $x \in [-1/e, 0]$. In particular, this implies that $B_c^* \sim \log K$ asymptotically when $K \to \infty$.

In the second case, when $B < B_c^*$, the solution resembles that of a propagating front with "velocity" v, where asymptotically $\psi_t(\tau) \equiv \psi(\tau - vt)$ with $v = B_c^* - B$. Thus, $v = \mathbb{E}[\tau(t) - \tau(t-1)]$ has the dimension a time and corresponds to the mean delay accumulated between two successive iterations of the model.

These results imply that the *order parameter* for the development of delays in time, v, undergoes a *second-order phase transition* when the control parameter B crosses B_c^*, with

$$v = \begin{cases} 0 & \text{if } B > B_c^* \\ B_c^* - B & \text{if } B < B_c^*. \end{cases} \tag{6}$$

In particular, we obtain that $v(B = 0) = B_c^*$, implying that the minimal buffer that must be applied to avoid any accumulation of delays corresponds precisely to the average delay accumulated in absence of buffers. Note also that α also has a different behavior above and below B_c^*, namely

$$\alpha = \begin{cases} 1 - \dfrac{W_0(-BKe^{-B})}{B} & \text{if } B > B_c^* \\ \alpha_c^* \equiv 1 - (B_c^*)^{-1} & \text{if } B < B_c^*, \end{cases} \tag{7}$$

which has a square-root singularity $(B - B_c^*)^{1/2}$ as $B \to$

K	B_c^*	α_c^*
2	2.67835	0.626636
3	3.28938	0.695991
4	3.69263	0.729190
5	3.99431	0.749644
6	4.23519	0.763883
7	4.43557	0.774550
8	4.60702	0.782940
9	4.75680	0.789775
10	4.88972	0.795489

TABLE I. The values of B_c^* and α_c^* from Eq. (5) for a few different values of K for the MF case.

B_c^* from above, suggesting that the transition of the same kind as the K-core percolation transition, which itself is akin to the Mode-Coupling Theory of glasses [13, 16].

We coin the term *temporal criticality* to describe this transition behavior. It is a critical transition, which we characterize below, but in the temporal dimension. The values of B_c^* and α_c^* for a few different values of K are shown in Table I.
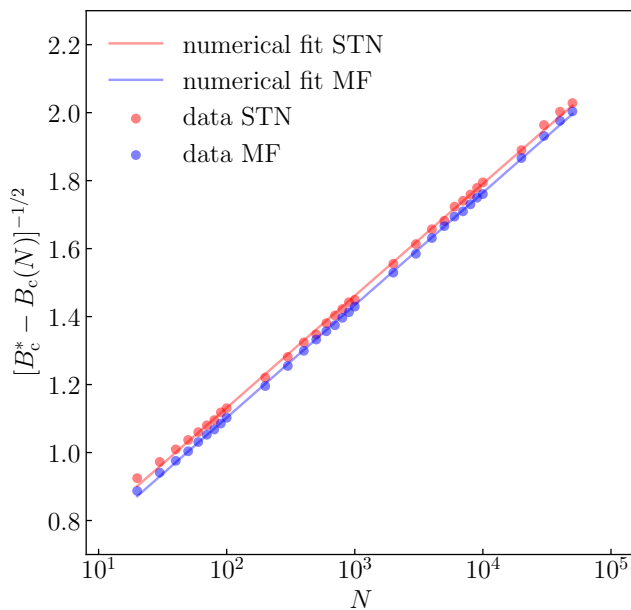

FIG. 3. Finite-N effects described by Eq. (8) for the critical buffer value $B_c(N)$ at $K = 5$, obtained from the order parameter analysis. The best linear fit values of (a, b) are $\approx (0.4723, 0.1432)$ (MF) and $\approx (0.4407, 0.1437)$ (STN). The dependence on $\ln N$ implies slow convergence to the asymptotic value B_c^*.

We used direct simulations of Eq. (2) for various values of N and K, in order to verify the above analytical results for the MF case. In Fig. 2(a) we show the behavior of the order parameter v as a function of the control parameter B using exponentially distributed noise for $N = 10,000$ and $K = 5$ (we note that the STN case

with exponential noise yields numerically indistinguishable results, although not shown here), from which we identify the critical buffer value. Correspondingly, the exponential tail behavior of $\psi(\tau) \equiv \psi_{t \to \infty}(\tau)$ we show in Fig. 2(b). In Fig. 2(c) we showcase the typical behavior of the mean delay per firm: when the buffer is smaller than the critical buffer, the mean delay per firm keeps accumulating without bound, while *avalanches* of all sizes appear spontaneously in the mean delay per firm when the buffer is smaller than the critical buffer, with no relation to the amplitude of the initial values of the noise term [i.e., $\varepsilon_i(t = 0)$]. Finally, in Fig. 2(d) we show the behavior of the order parameter v as a function of B, identify B_c from it.

We also note that changing the distribution of the noise to, for example, a folded Gaussian with $P(\varepsilon) = \mathbf{1}_{\varepsilon > 0} \sqrt{2/\pi} \exp(-\varepsilon^2/2)$, yields qualitatively similar results. We expect the presence of a heavy (power-law) tail will change the nature of the transition but henceforth we limit ourselves only to exponentially distributed noise in this paper.

In the language of interfaces and of the B-KPZ equation, the delay accumulating transition reported above corresponds to a depinning transition [11, 12], which appear in many different contexts (domain walls in magnets, fracture fronts, yielding, etc.), see e.g. [17–20] and refs. therein.

C. Finite-N effects

It is clear from Fig. 2(c-d) that the values of B_c and α_c for $N = 10,000$ and $K = 5$ do not match the analytical solution provided in Table I. We reason in Fig 3 that this is caused by finite-N effects. Indeed, we find that the $B_c(N)$ data for both the MF and the STN cases can been fitted very well with a function of the type

$$B_c(N) = B_c^* - \frac{1}{(a + b \ln N)^2}. \qquad (8)$$

One plausible explanation for the $\ln N$-dependence can be the "small-world phenomenon": since the inputs of every firm comes from K randomly chosen firms at every time step for the MF case, on average the input-output links among all possible firms have been established within $\mathcal{O}(\ln N)$ time steps, which is the diameter of a sparse random graph [21, 22]. The same can be argued for STN as well, but additional constraints (such as clustering within the supply chain, or any sector structure) can make this effect more pronounced. Remarkably, Eq. (8) predicts a $(\ln N)^{-2}$ asymptotic convergence for large N, which is strongly reminiscent of the classic result of Brunet & Derrida [23] for the finite size correction to the velocity of traveling fronts that appear in the analytical solution of our problem on a tree-like structures (SI E and [24]). Although the precise mathematical connection is unclear to us at this stage, it is not unreasonable to surmise that such a connection indeed exists.

III. CHARACTERIZING TEMPORAL CRITICALITY

A. Temporal correlations

In critical phenomena one expects (power-law) diverging correlation lengths as the control parameter gets closer to the critical value in the disordered phase. For temporal criticality, we expect diverging correlation lengths *in time* as $B \to B_c^*$ from above. There is however a subtlety: correlations in the delays of individual firms decorrelate within times of $O(1)$. For the MF case, to which we confine ourselves in Sec. III, this should however not come as a surprise since the temporal adjacency matrix $\mathbf{A}$ is composed randomly at every time step.
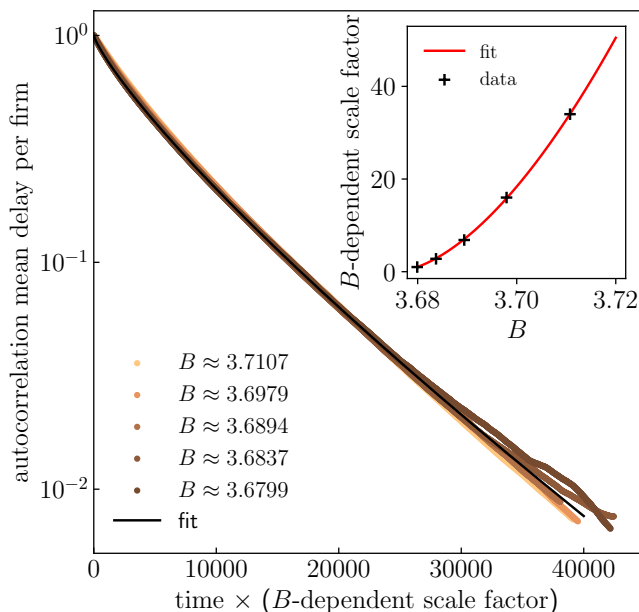

FIG. 4. Autocorrelation function of mean delay per firm for $N = 10,000$ and $K = 5$ for the MF case. The data have been collapsed to the reference curve ($B \approx 3.6799$) by stretching the x-axis by B-dependent scale factors. A stretched exponential of the form $\exp[-(t/t_{\mathrm{ref}})^\beta]$ in temporal depth t, with best-fitted values $t_{\mathrm{ref}} \approx 5835.6$ and $\beta \approx 0.823$ provides an excellent fit to the collapsed data. Inset: these scale factors are fitted by the function (9), showcasing that the correlation length in the temporal domain diverges as a power-law when B approached B_c^* from above. See text for details.

That said, from Figs. 2(c-d) we expect the signs of diverging correlation lengths to be picked up by the mean delay per firm, defined as $\sum_i \tau_i / N$. This is explored in Fig. 4 for $N = 10,000$ and $K = 5$, where we collapse the temporal autocorrelation function of the mean delay per firm by stretching the x-axis by B-dependent scale factors for five different B-values. These scale factors are then plotted in the inset of Fig. 4 (symbols) and fitted

with a curve

$$B\text{-dependent scale factor} = \frac{[B - B_c(N)]^\gamma}{[B_{\mathrm{ref}} - B_c(N)]^\gamma}, \quad (9)$$

which we have (arbitrarily) normalized using $B_{\mathrm{ref}} = 3.6799$. From such a fit we obtain $B_c(N) \approx 3.6755$ and $\gamma \approx 1.6936$. In other words, Fig. 4 showcases that the correlation time indeed diverges as a power-law when B approaches the critical value from above.

We note that such a data collapse is very sensitive to the fitting parameters $B_c(N)$ and γ — especially to $B_c(N)$ — this is a standard method used for identifying critical exponents with a high degree of numerical precision [25]. We also note that the shape of the collapsed curves in Fig. 4 suggests that the correlation functions do not decay as a pure exponential: numerically, we find that a stretched exponential, with a stretching exponent $\beta \approx 0.823$, produces an excellent fit to the collapsed curve.

As we have seen above, exponent γ, governing the divergence of the relaxation time as B_c^* is approached, is very precisely determined by our numerical data. However, perhaps surprisingly in view of the usual universality property of critical exponents, we have found that γ depends on, e.g., the connectivity of the network K. For example, the data collapse of the autocorrelation of mean delay per firm for $N = 10,000$ and $K = 7$ is also excellent and yields $B_c(N) \approx 4.0441$ and $\gamma \approx 1.745$, distinctly different from the value $\gamma \approx 1.6936$ obtained for $K = 5$. Other exponents, such as stretching exponent β or the exponent governing the avalanche persistence time reported in the next section, *are* universal. Such a coexistence of universal and non universal exponents is, as already suggested above, reminiscent of a similar situation for the Mode-Coupling Theory of glasses [13]. There too, the exponent γ describing the divergence of the relaxation time as the glass transition is approached is non universal, whereas the Debye-Waller factor has a universal square-root singularity in the glass phase.

B. Delay avalanches

Figures 2(c-d) suggest that we define and analyze delay "avalanches", in close analogy with avalanches appearing at depinning, fracture or yielding transitions [17, 19, 20]. Since delays can never be negative, delays that are above a certain threshold are of particular interest. In fact, the buffer B is such a natural threshold, since delays below B at a given time step gets absorbed by the buffer. Based on Figs. 2(c-d) we therefore again consider mean delay per firm, and define as avalanche those cases when the mean delay per firm is $> B$. This brings two aspects of avalanches in focus: (i) *avalanche persistence times*, defined as the time the mean delay stays above B once it becomes larger than B, and (ii) *avalanche size*, defined as the area under the avalanche curve over the persistence times above the threshold B.
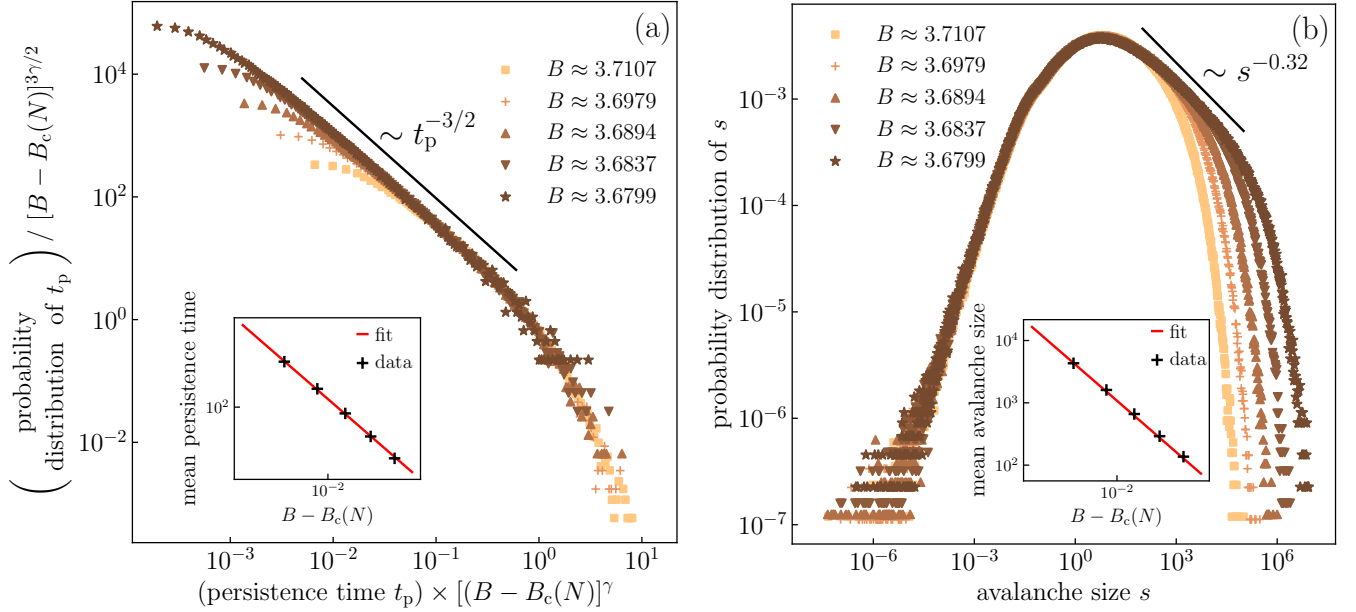
FIG. 5. Probability distribution of avalanche persistence times (a), and of avalanche sizes (b) for the MF case, with $N = 10,000$ and $K = 5$. Panel (a): an excellent data collapse is obtained for the probability distribution of avalanche persistence times by scaling the x- and the y-axes by $[B - B_c(N)]^{-\gamma}$ and $[B - B_c(N)]^{-3\gamma/2}$ respectively, with the $B_c(N) \approx 3.6755$ and $\beta \approx 1.6936$, determined from Fig. 4. Inset (a): mean persistence times for the five B-values shown in the main plot; the red line corresponds to $\approx 2.355[B - B_c(N)]^{-\gamma/2}$, implying that the mean avalanche persistence time diverges $\sim [B - B_c(N)]^{-\gamma/2}$ (as it must given the data collapse of the main plot) when $B \to B_c(N)$ from above. Panel (b): the probability distribution of avalanche sizes is independent of B at the lower end of the avalanche size, but at the higher end it behaves with an (apparent) power-law with exponent ≈ -0.32, with the power law lasting deeper into the avalanche size as $B \to B_c(N)$ from above. Inset (b): mean avalanche sizes for the five B-values shown in the main plot; the red line $\approx 0.443[B - B_c(N)]^{-\gamma}$ is a numerically obtained fit to the data, implying that the mean avalanche size diverges $\sim [B - B_c(N)]^{-\gamma}$ as $B \to B_c(N)$ from above. See also main text.

The probability distributions of persistence times and avalanches sizes for $N = 10,000$ and $K = 5$ for the MF case are shown in Figs. 5(a) and (b) respectively. Using $B_c(N) \approx 3.6755$ and $\gamma \approx 1.6936$ as found in Fig. 4 we obtain an excellent collapse for the probability distributions of the persistence times: Fig. 5(a) shows that long persistence times become increasingly likely as a power-law with an exponent $\approx -3/2$, corresponding to the return time probability density of an unbiased random walk, while the typical time of avalanches diverges as $[B - B_c(N)]^{-\gamma}$. Note that this implies that the *mean avalanche time* diverges more slowly, as $[B - B_c(N)]^{-\gamma/2}$, due to the explosion of the number of "small" avalanches.

Similarly, large avalanches also become increasingly likely as a power-law with an (apparent) exponent ≈ -0.32, with the power-law behavior holding on for progressively larger avalanche sizes as $B \to B_c$ from above, although the probability distribution of avalanche sizes remains independent of the value of B [Fig. 5(b)]. Finally, using a numerical fit to the data the mean avalanche size is seen to increase $\sim [B - B_c(N)]^{-\gamma}$ [inset of Fig. 5(b)]. We note that these results are in agreement with the qualitative picture of Fig. 2(c-d).

C. Fluctuations in mean delay per firm

We also characterized the fluctuations in the mean delay per firm close to criticality. For this, we introduced the fluctuations for a run over the time interval $[\![0, T]\!]$ as

$$\Delta\tau(t) \equiv \frac{1}{N}\sum_i [\tau_i(t) - vt] \quad \text{for } 0 \le t \le T, \qquad (10)$$

where v was computed from a linear regression on the mean delay per firm $\sum_i \tau_i/N$ data over the time interval $[\![0, T]\!]$. We then computed the variogram of the fluctuations, defined as

$$\mathcal{V}(\ell) \equiv \text{Var}\left[\Delta\tau(t + \ell) - \Delta\tau(t)\right], \qquad (11)$$

where the variance is computed over t.

For purely diffusive processes, $\mathcal{V}(\ell) \propto \ell$. The variogram is plotted in Fig. 6 (main graph) for several B-values above $B_c(N)$, where we see that the variogram is initially linear in ℓ, but departs from the linear trend at larger ℓ-values. Moreover, the point of departure from the linear trend occurs at progressively larger values of ℓ as B approaches $B_c(N)$. In other words, the mean delay per firm follows a biased random-walk close to criticality: on top of the average drift v, the mean delay per firm

evolves completely randomly at each time step. This behavior is in line with the spectral density of fluctuations $S(f)$, defined as

$$S(f) \equiv \left| \sum_{t=1}^{T} \Delta\tau(t) e^{-2i\pi f t/T} \right|^2 , \qquad (12)$$

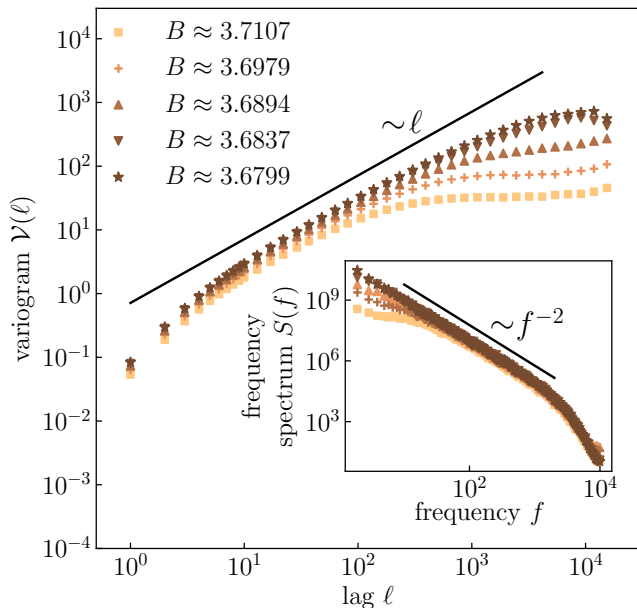becoming closer to f^{-2} for progressively smaller values of f as B approaches $B_c(N)$ Fig. 6 (inset).

FIG. 6. Main graph: Variogram of fluctuations in mean delay per firm (the same B-values used in Fig. 5, using also the same color scheme). Inset: corresponding spectral density of fluctuations $S(f)$. See text for details.

IV. CRITICALITY ON REAL-WORLD TEMPORAL NETWORKS

In contrast to the stylized models we have analyzed so far, in temporal networks describing real-world processes [e.g., Fig. 1(a)], delays do not develop at discrete time steps. Neither are the firms located on a "lattice", as shown in Figs. 1(b-c), nor are the buffers of the same magnitude ($= B$) everywhere. Therefore, in order to bridge the gap between stylized models and the real world, we investigate the development of delays on two real-world temporal networks and demonstrate the

proof-of-principle applicability of the concept temporal criticality to the real world.

Many real-world operational data are often too coarse or not easily accessible. Firm-to-firm input-output production network data, for example, is often not available at product level, with corresponding buffers, and/or proprietary. We therefore choose temporally-resolved contact data among pupils from a high school [26] and employees at a workplace [27], both of which are publicly available from sociopatterns.org (data description in SI C). The contacts are traced at discrete time steps (at 20 seconds interval), and the temporal network is highly disordered, i.e., there are large variations in the temporal adjacency matrix $\mathbf{A}(t)$, which are directly taken from the empirical data.

We "event mapped" [28, 29] these temporal networks to suit our purpose: an example is shown in Fig. 7(a), wherein contacts among individual agents (pupils, employees; each agent with a unique alphanumeric tag) at discrete time steps are shown by thick red lines. Every connected component of the network is termed "an event"; once the events at every time step is constructed, in the temporal networks the agents can be seen as moving from one event to another across time steps. Note that the number of agents entering a specific event must also be equal to the number of agents leaving that event, albeit, unlike the case of STNs, the number of agents per event is not a constant (neither is the number of events taking place per time step).

We simulated delay development [Eq. (2)] on these temporal networks for uniform buffer B. Delays develop in a manner analogous to Fig. 1(b): delays are carried by agents, and the delay of an event i at time t is the maximum of the delays of the agents entering that event plus an exponentially distributed random noise term ε_i with exponent unity. Note however the presence of single-agent "events" [colored blue in Fig. 7(b)]: for such events no noise term is added, as they are considered to be temporarily outside the system (e.g., a transport crew having a lunch break).

The corresponding v vs B plots, analog of Fig. 2(a) are shown in Fig. 7(b) (main graph), and with a logarithmic y-axis (inset). Evidently, there are critical transitions for both data sets, as the v vs B curves exhibit a power-law singularity (with a power larger than 1) in $(B_c - B)$, signified by $d(\log v)/d(\log B)$ approaching infinity from the left, allowing us to cleanly identify the corresponding critical values B_c. We note that disorder increases the order of transition has been found elsewhere [19, 30].
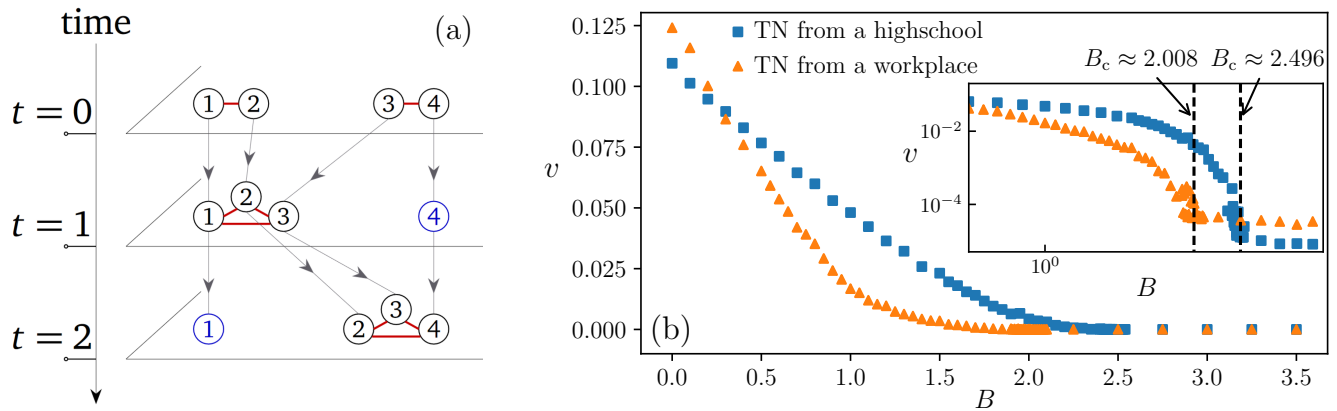
FIG. 7. (a) An example event representation for a real-world temporal network, consisting of four agents, numbered 1 through 4. The contact links among the agents at any time step is denoted by a thick red line, and each connected component — such as 1-2 and 3-4 at time step 0 constitutes an event. An event can consist of a single agent as well, denoted by a blue agent node and blue outgoing connections. Single-agent events do not propagate delay according to Eq. 2, because they miss the noise term $\epsilon_i(t)$. Once the events are constructed at all time steps, agents can be seen to move from one event to another across time steps. (b) The v vs B graph for the two real-world temporal networks (TNs), the inset showing the same data as in the main graph, but with double logarithmic axes. At the B-values noted in the inset by dashed lines, the slopes of $\log v$ sharply approach infinity; these we identify as the critical buffer B_c. One can fit the singularity at B_c as a power-law $(B_c - B)^\zeta$ with $\zeta \approx 5/2$.

In contrast to Fig. 2(a), the transitions are however not only smooth in v vs. B plots [e.g., v does not have a discontinuous first derivative in B as in Fig. 2(a)], but we also find them taking place at lower values of B_c than expected for STNs with similar numbers of agents. In SI D we argue that this is likely caused by the "sparsity" rather than by the "heterogeneity" in the temporal network topology (the terms are defined in SI D).

V. CONCLUSION AND DISCUSSIONS

The value of goods and services depends on the timeliness of their provisions; for example, the value of a ride service is not only to go from A to B but to also do so on time. Similarly, the economic value of energy or a glass of water is also determined by whether they are available on time. System operators that provide these goods and services, on the one hand, have therefore integrally adopted timeliness as a quality standard, and on the other hand, are continuously striving to improve cost- and time-efficiencies in order to achieve superior operational results. We have captured the competition between achieving timeliness and the strive for efficiency – and more generally between efficiency and resilience [1] – in terms of a stylized model on temporal networks with a delay-mitigating temporal buffer B: more buffer translates to higher inefficiency, but more adherence to timeliness and stability. With B as the control parameter, the model exhibits *temporal criticality*, a novel form of phase transition *in time* that occurs at a critical value of B. Above this critical value, delay avalanches of all sizes appear spontaneously. For the stylized model we

have characterized these avalanches and have identified the corresponding critical exponents.

We have also shown that real-world temporal networks, which are not a lattice, also exhibit temporal criticality. Nevertheless, several challenges still exist for a meaningful translation of temporal buffers in our model to the real world. First, temporal buffers are an aggregate of diverse measures in reality. For example, a production planner in a firm can increase temporal buffers by producing faster or in overtime, by increasing inventories, securing more suppliers for the same input, improving (electronic) procurement systems, changing product designs to reduce exposure to critical inputs, and so on [5]. Each of these measures comes with its own possibilities and limitations in terms of efficiency and buffering dynamics. Second, many firms have extensive production planning and operations research departments that tackle the trade-off between cost efficiency and delivery security on time [9]. However, this research and planning is mostly limited to units within the firm, and to other firms with direct contractual links (suppliers and customers). The supplier of the supplier is already less foreseeable, not to speak of a supplier three or four links away on another continent [31]. Lastly, an important element that our simplified model does not capture is the heterogeneity in time delays and inventory levels, a point that was shown to be important in the model described in [6]. The complex interactions among firms, simultaneously trying to anticipate the actions of other firms, can lead to emergent system dynamics, as demonstrated by the 'bullwhip effect', illustrated through the well-known 'beer game' [32]. Hence, both the heterogeneous composition of temporal buffers and their myopic adjustment

can have very different implications for emergent behavior and temporal criticality.

Of particular interest for the applicability of our model to real STSs is how relatively small and/or local events can lead to avalanches and system-wide disruptions, such as the cancellation of all train rides to reboot scheduling [33], a worldwide supply chain blockage due to natural disasters [34], or even a full-blown economic crisis, such as the global financial crisis in 2008 that emanated from the cracks in subprime loans, which represented a puny fraction of the US economy [35]. Following the early work of Bak et al. [36], one might argue that the tendency of efficiency-driven operators to self-organize into (temporal) criticality explains why financial markets and economies are more volatile than expected based on economic equilibrium models with rational expectations [37]. This well-known phenomenon is referred to as the "excess volatility puzzle", or the "small shocks, large business cycle puzzle" [35, 38], the explanation of which, despite numerous attempts, remains elusive (see e.g. [10, 39] and [40] for a recent review). The "temporal criticality" developing on firm-to-firm networks may be a potent cause for an imbalance in demand and supply, leading to large scale volatility in economic output and in corresponding prices of goods and services. This is in fact very visible in agent-based economic models [8, 10, 41], and aligned with empirical evidence of firms with low inventories being less resilient in a crisis [42]. Thus, when operating close to temporal criticality, the network is highly sensitive to delays, which may explain the well-documented and persistent existence of bubbles and crashes in prices (see, e.g., [43]).

Going beyond STSs, the concept of temporal criticality may be a promising approach for other input-output systems with temporal buffers and incentives for improving efficiency like, e.g. distributed computing systems or task schedulers. In the tradition of physics contributing to neuroscience [44], our model may also be a novel avenue for self-organizing neural networks with temporal signal transmission along structural connections, critical buffers in neural excitability and activity states, and efficiency incentives for minimizing energy and/or surprises (see, e.g., [45] and [46]).

Author contributions. J-PB and DP conceptualized temporal criticality. J-PB, PLD, JM, DP, FPP and MR analyzed temporal criticality. All authors contributed to the manuscript.

[1] J. Moran, F. P. Pijpers, U. Weitzel, J.-P. Bouchaud, and D. Panja, Temporal criticality in socio-technical systems, arXiv:2307.03546 (2023).
[2] M. M. Dekker and D. Panja, Cascading dominates large-scale disruptions in transport over complex networks, PLOS One **16**, e0246077 (2021).
[3] V. Giannikas, A. Ledwoch, G. Stojković, P. Costas, A. Brintrup, A. A. S. Al-Ali, V. K. Chauhan, and D. McFarlane, A data-driven method to assess the causes and impact of delay propagation in air transportation systems, Transportation Research Part C: Emerging Technologies **143**, 103862 (2022).
[4] A. Ledwoch, A. Brintrup, J. Mehnen, and A. Tiwari, Systemic risk assessment in complex supply networks, IEEE Systems Journal **12**, 1826 (2016).
[5] A. Brintrup and A. Ledwoch, Supply network science: Emergence of a new perspective on a classical field, Chaos: An Interdisciplinary Journal of Nonlinear Science **28**, 10.1063/1.5010766 (2018).
[6] C. Colon and M. Ghil, Economic networks: Heterogeneity-induced vulnerability and loss of synchronization, Chaos: An Interdisciplinary Journal of Nonlinear Science **27**, 126703 (2017).
[7] T. A. Press, Ship still stuck in suez canal as backlog grows to 150 other ships (2021), accessed: September 14 2023.
[8] C. Colon, S. Hallegatte, and J. Rozenberg, Criticality analysis of a country's transport network via an agent-based supply chain model, Nature Sustainability **4**, 209 (2020).
[9] E. E. Kosasih and A. Brintrup, Reinforcement learning provides a flexible approach for realistic supply chain safety stock optimisation, IFAC-PapersOnLine **55**, 1539 (2022).
[10] T. Dessertaine, J. Moran, M. Benzaquen, and J.-P. Bouchaud, Out-of-equilibrium dynamics and excess volatility in firm networks, Journal of Economic Dynamics and Control **138**, 104362 (2022).
[11] M. A. Munoz and T. Hwa, On nonlinear diffusion with multiplicative noise, Europhysics Letters **41**, 147 (1998).
[12] H. Hinrichsen, Non-equilibrium critical phenomena and phase transitions into absorbing states, Advances in Physics **49**, 815 (2000).
[13] W. Götze, *Complex dynamics of glass-forming liquids: A mode-coupling theory*, Vol. 143 (Oxford University Press, USA, 2009).
[14] P. Holme and J. Saramäki, Temporal networks, Physics Reports **519**, 97 (2012).
[15] P. Holme and J. Saramäki, *Temporal networks* (SpringerLink, 2013).
[16] M. Sellitto, G. Biroli, and C. Toninelli, Facilitated spin models on bethe lattice: Bootstrap percolation, mode-coupling transition and glassy dynamics, Europhysics Letters **69**, 496 (2005).
[17] A. Rosso, P. Le Doussal, and K. J. Wiese, Avalanche-size distribution at the depinning transition: A numerical test of the theory, Physical Review B **80**, 144204 (2009).
[18] E. Bouchaud, Scaling properties of cracks, Journal of Physics: Condensed Matter **9**, 4319 (1997).
[19] J. Lin, E. Lerner, A. Rosso, and M. Wyart, Scaling description of the yielding transition in soft amorphous solids at zero temperature, Proceedings of the National Academy of Sciences **111**, 14382 (2014).
[20] L. Ponson and N. Pindra, Crack propagation through disordered materials as a depinning transition: A critical

test of the theory, Physical Review E **95**, 053004 (2017).

[21] D. Fernholz and V. Ramachandran, The diameter of sparse random graphs, Random Structures and Algorithms **31**, 482 (2007).

[22] F. Chung and L. Lu, The diameter of sparse random graphs, Advances in Applied Mathematics **26**, 257 (2001).

[23] E. Brunet and B. Derrida, Shift in the velocity of a front due to a cutoff, Physical Review E **56**, 2597 (1997).

[24] B. Derrida and H. Spohn, Polymers on disordered trees, spin glasses, and traveling waves, Journal of Statistical Physics **51**, 817 (1988).

[25] M. E. J. Newman and G. T. Barkema, *Monte Carlo methods in statistical physics* (Oxford University Press, Oxford, 1999).

[26] R. Mastrandrea, J. Fournet, and A. Barrat, Contact patterns in a high school: A comparison between data collected using wearable sensors, contact diaries and friendship surveys, PLOS ONE **10**, 1 (2015).

[27] M. Génois, C. L. Vestergaard, J. Fournet, A. Panisson, I. Bonmarin, and A. Barrat, Data on face-to-face contacts in an office building suggest a low-cost vaccination strategy based on community linkers, Network Science **3**, 326 (2015).

[28] M. M. Dekker, R. D. Schram, J. Ou, and D. Panja, Hidden dependence of spreading vulnerability on topological complexity, Physical Review E **105**, 054301 (2022).

[29] M. M. Dekker, T. F. Blanken, F. Dablander, J. Ou, D. Borsboom, and D. Panja, Quantifying agent impacts on contact sequences in social interactions, Scientific Reports **12**, 3483 (2022).

[30] S. Roux and H. J. Herrmann, Disorder induced nonlinear conductivity, Europhysics Letters **4**, 1227 (1987).

[31] P. Wichmann, A. Brintrup, S. Baker, P. Woodall, and D. McFarlane, Towards automatically generating supply chain maps from natural language text, IFAC-PapersOnLine **51**, 1726 (2018).

[32] J. Sterman, Modeling managerial behavior: Misperceptions of feedback in a dynamic decision making experiment, Management Science **35**, 321 (1989).

[33] M. M. Dekker *et al.*, A next step in disruption management: combining operations research and complexity science, Public Transport **14**, 5 (2021).

[34] C. Shughrue, B. Werner, and K. C. Seto, Global spread of local cyclone damages through urban trade networks, Nature Sustainability **3**, 606 (2020).

[35] B. S. Bernanke, T. F. Geithner, and H. M. Paulson Jr., *Firefighting: the financial crisis and its lessons* (Penguin, 2019).

[36] P. Bak, K. Chen, J. Scheinkman, and M. Woodford, Aggregate fluctuations from independent sectoral shocks: self-organized criticality in a model of production and inventory dynamics, Ricerche economiche **47**, 3 (1993).

[37] J. Moran and J.-P. Bouchaud, May's instability in large economies, Physical Review E **100**, 032307 (2019).

[38] B. S. Bernanke, M. Gertler, and S. Gilchrist, The financial accelerator and the flight to quality, The Review of Economics and Statistics **78**, 1 (1996).

[39] X. Gabaix, The granular origins of aggregate fluctuations, Econometrica **79**, 733 (2011).

[40] V. M. Carvalho and A. Tahbaz-Salehi, Production networks: A primer, Annual Review of Economics **11**, 635 (2019).

[41] A. Pichler and J. D. Farmer, Simultaneous supply and demand constraints in input–output networks: the case of covid-19 in germany, italy, and spain, Economic Systems Research **34**, 273 (2021).

[42] R. Lafrogne-Joussier, J. Martin, and I. Mejean, Supply shocks in supply chains: Evidence from the early lockdown in china, IMF Economic Review **71**, 170 (2022).

[43] U. Weitzel, C. Huber, J. Huber, M. Kirchler, F. Lindner, and J. Rose, Bubbles and financial professionals, The Review of Financial Studies **33**, 2659 (2020).

[44] C. W. Lynn and D. S. Bassett, The physics of brain network structure, function and control, Nature Reviews Physics **1**, 318 (2019).

[45] T. Isomura, K. Kotani, Y. Jimbo, and K. J. Friston, Experimental validation of the free-energy principle with in vitro neural networks, Nature Communications **14**, 4547 (2023).

[46] M. Khona and I. R. Fiete, Attractor and integrator networks in the brain, Nature Reviews Neuroscience **23**, 744 (2022).

SI A: Evolution of delays for exponentially distributed noise

We assume that $\varepsilon_i(t)$ is an i.i.d. random variable, taken from the distribution $P(\varepsilon) = \mathbf{1}_{\varepsilon>0}\exp(-\varepsilon)$. Let us denote the probability distribution function (pdf) of the delays at the time step t by $\psi_t(\tau)$, with $\psi_0(\tau) = P(\tau)$.

The way to construct ψ_{t+1} from ψ_t is by taking K samples from the pdf ψ_t. As explained in Eq. (3) at time step $t+1$ a firm can have an output delay τ in two distinct ways: (i) when the max of the K chosen samples from ψ_t have a delay equal to $\tau + B - \varepsilon$, and (ii) when the max of the K chosen samples from ψ_t have a delay $< B$. In the first case, B amount of delay gets absorbed from the maximum and ε gets added to the delay of from the noise term. Then we need to integrate the noise term ε from 0 to τ. In the second case, $\psi_{t+1}(\tau) \sim \exp(-\tau)$, inherited from the distribution of the noise itself. In other words,

$$\psi_{t+1}(\tau) = \int_0^\tau d\varepsilon\ \exp(-\varepsilon)\ \underbrace{[\text{pdf of max of the } K \text{ chosen samples has value } (\tau + B - \varepsilon)]}_{Q(\tau+B-\varepsilon)}$$

$$+ \exp(-\tau)\int_0^B du\ \underbrace{[\text{pdf of max of the } K \text{ chosen samples has value } u]}_{Q(u)} \tag{A1}$$

We choose K samples from the probability distribution to satisfy that the maximum of them equals u. So we choose one of them with a delay u, and the rest $(K-1)$ samples I choose with delays $\leq u$. Moreover, the one with a delay u can be chosen in K distinct ways, meaning that

$$Q(u) = K\,\psi_t(u)\,[1 - \Psi_t(u)]^{K-1}, \tag{A2}$$

where $\Psi_t(u)$ given by

$$\Psi_t(u) = \int_u^\infty du'\ \psi_t(u'), \tag{A3}$$

leading to

$$\psi_t(u) = -\frac{d}{du}\Psi_t(u). \tag{A4}$$

This means

$$Q(u) = \frac{d}{du}[1 - \Psi_t(u)]^K \quad \text{and} \quad Q(\tau + B - \varepsilon) = -\frac{d}{d\varepsilon}[1 - \Psi_t(\tau + B - \varepsilon)]^K. \tag{A5}$$

Using Eq. (A5) in Eq. (A1) we get

$$\psi_{t+1}(\tau) = \exp(-\tau)\underbrace{\int_0^B du\ \frac{d}{du}[1 - \Psi_t(u)]^K}_{=[1-\Psi_t(B)]^K,\ \text{since } \Psi_t(0)\,=\,1}\ -\int_0^d d\varepsilon\ \exp(-\varepsilon)\frac{d}{d\varepsilon}[1 - \Psi_t(\tau + B - \varepsilon)]^K. \tag{A6}$$

We do an integration by parts of the second term to write

$$\psi_{t+1}(\tau) = [1 - \Psi_t(B)]^K\exp(-\tau) - \exp(-\varepsilon)\left[1 - \Psi_t(\tau + B - \varepsilon)\right]^K\Big|_{\varepsilon=0}^{\varepsilon=\tau} - \int_0^\tau d\varepsilon\ \exp(-\varepsilon)\left[1 - \Psi_t(\tau + B - \varepsilon)\right]^K$$

$$= [1 - \Psi_t(\tau + B)]^K - \int_0^\tau du\ \exp[-(\tau - u)]\,[1 - \Psi_t(u + B)]^K. \tag{A7}$$

A first order derivative of Eq. (A7) wrt τ yields

$$\psi_{t+1}'(\tau) = -K[1 - \Psi_t(\tau + B)]^{K-1}\,\Psi_t'(\tau + B) - \underbrace{\left[[1 - \Psi_t(\tau + B)]^K - \int_0^\tau du\ \exp[-(\tau - u)]\,[1 - \Psi_t(u + B)]^K\right]}_{=\,\psi_{t+1}(\tau)\ \text{from Eq. (A7)}}, \tag{A8}$$

or in surprisingly simple form,

$$\psi'_{t+1}(\tau) + \psi_{t+1}(\tau) = -K[1 - \Psi_t(\tau + B)]^{K-1} \Psi'_t(\tau + B), \tag{A9}$$

which reduces to, using Eq. (A4),

$$\Psi''_{t+1}(\tau) + \Psi'_{t+1}(\tau) = K[1 - \Psi_t(\tau + B)]^{K-1} \Psi'_t(\tau + B). \tag{A10}$$

SI B: Asymptotic solution of delay evolution with exponential noise

1. Case I: $B > B_c^*$, time-independent stationary solution

Let us look for a stationary, i.e. time independent, solution of Eq. (A10) at large time. Such a function $\Psi(\tau)$ satisfies

$$\Psi''(\tau) + \Psi'(\tau) = K[1 - \Psi(\tau + B)]^{K-1} \Psi'(\tau + B). \tag{B1}$$

Note that in the limit $B \to \infty$ the right-hand side of this equation is equal to 0. This is trivial, as in that limit the evolution given in Eq. (2) imposes $\tau_i(t) = \varepsilon_i(t)$, implying that $\Psi(\tau) = e^{-\tau} \mathbf{1}_{\tau>0}$ is the correct time-independent solution.

Another way to see this is to rewrite Eq. (B1) as

$$0 = -\frac{\partial}{\partial \tau} \left[\Psi' + \Psi + [1 - \Psi(\tau + B)]^K \right], \tag{B2}$$

which means that:

$$\Psi' + \Psi + [1 - \Psi(\tau + B)]^K = c. \tag{B3}$$

Using that $[1 - \Psi(\tau + B)] \approx 1$ for large values of the argument (i.e. large B), this reduces to:

$$\Psi' + \Psi = c - 1 \tag{B4}$$

defining for convenience $u \equiv \Psi - \Psi(0)$ then we have an inhomogeneous initial value problem:

$$\begin{aligned} u' + u &= c - 1 - \Psi(0) \equiv \gamma \\ u(0) &= 0 \end{aligned} \tag{B5}$$

which has the unique solution:

$$u = \Psi - \Psi(0) = \gamma \left[1 - e^{-\tau} \right]. \tag{B6}$$

In order for $\Psi \to 0$ for large values of its argument, the constant of integration must be $\gamma = -\Psi(0)$ and therefore

$$\Psi = \Psi(0)e^{-\tau}. \tag{B7}$$

We may then restore a finite B in Eq. (B3). Keeping the lowest-order terms, the correction to the differential equation reads:

$$\Psi' + \left[1 - Ke^{-B}\right] \Psi = c - 1. \tag{B8}$$

This correction is important because it shows that this improved, but still approximate, solution behaves as $\Psi \propto e^{-\alpha \tau}$ with $\alpha < 1$. Therefore, using $\Psi \propto e^{-\alpha \tau}$ is a reasonable approximation which can be used to obtain further constraints to our problem. Using $\Psi \propto e^{-\alpha \tau}$ in Eq. (B3) and keeping only the lowest-order terms leads to

$$1 - \alpha = K \exp(-B\alpha). \tag{B9}$$

A solution of Eq. (B9) can only exist if $\alpha < 1$ since the right-hand side of the equation, which we denote by $f(\alpha) \equiv Ke^{-B\alpha}$ on Fig. 8, is a positive quantity.

In order to solve Eq. (B9) we multiply each side by $-B$ and, denoting $w = -B(1 - \alpha)$, notice that it takes the form

$$we^w = -BKe^{-B} \Leftrightarrow B(1 - \alpha) = W(-BKe^{-B}) \tag{B10}$$

which determines α. Here $W(x)$ is the Lambert function, i.e. the solution of $We^W = x$. No solution exists for $x < -1/e$, while for $x \in [-1/e, 0]$ the Lambert function has two branches, shown on the left panel of Figure 8 $W_0(x) \in [0, -1]$ and $W_{-1}(x) \in [-1, -\infty]$. They meet at $W_0(-1/e) = W_{-1}(-1/e) = -1$. Hence, when $BKe^{-B} > 1/e$ there are no solutions for α, while for $BKe^{-B} < 1/e$ two solutions appear.
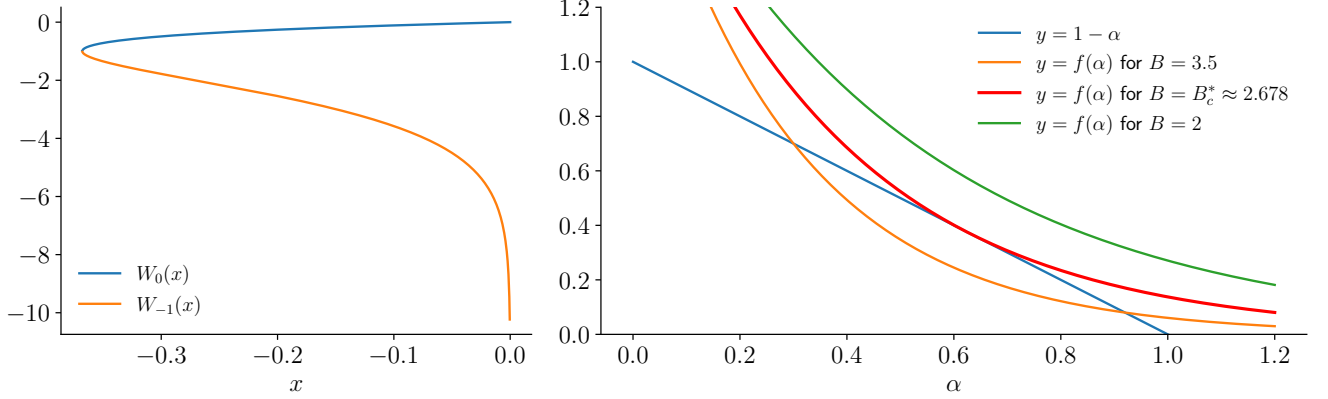

FIG. 8. Left: the two branches of the Lambert function. To recover the right limit $\alpha \to 1$ as $B \to \infty$ for fixed K, the W_0 branch should be used to find the value of α_c^*, while the other branch should be used to obtain the value of B_c^*. Right: Plots of $f(\alpha)$ for $K = 2$ and several values of B. The corresponding critical values are $B_c^* \approx 2.678$ and $\alpha_c^* \approx 0.627$.

Varying B at fixed $K > 1$, there is thus a transition at $B = B_c^*$, which satisfies

$$B_c^* e^{-B_c^*} = \frac{1}{eK}, \tag{B11}$$

leading in turn to an unique solution for α, namely

$$1 - \alpha_c^* = 1/B_c^*. \tag{B12}$$

Equation (B11) is itself solved using the Lambert function, as $B_c^* = -W(-1/(eK))$. Because $K > 1$, two roots are possible, but for $B \gg 1$ the solution should read $\psi(\tau) \approx e^{-\tau}$, meaning that we should *decrease* B until we reach the transition. Hence, we must choose the *largest* root of (B11), so that the critical point is given by

$$B_c^* = -W_{-1}(-1/(eK)) > 1 \tag{B13}$$

as displayed in the main text.

For $B \geq B_c^*$ there is thus a time independent solution for $\psi(\tau)$. In that phase one has then $BKe^{-B} < 1/e$ and the value of α is given by (B10) with $W = W_0$ (which has the correct limit $\alpha = 1$ for $B \to +\infty$, while W_{-1} gives $\alpha = 0$).

a. **Square-root singularity** we may also see how $\alpha - \alpha_c^*$ behaves compared with $B - B_c^*$. Writing $\alpha = \alpha_c^* + \eta$ and $B = B_c^* + \epsilon$ into Eq.(B9) and keeping terms of first order in ϵ and up to second order in η, we obtain

$$1 - \alpha_c^* - \eta \approx \frac{1}{B_c^*} \exp(-B_c^* \eta - \alpha_c^* \epsilon)$$
$$\approx \frac{1}{B_c^*} \left[1 - B_c^* \eta - \alpha_c^* \epsilon + \frac{1}{2} \left(B_c^{*2} \eta^2 + \alpha_c^{*2} \epsilon^2 \right) \right] \tag{B14}$$
$$\approx 1 - \alpha_c^* - \eta - \frac{\alpha_c^*}{B_c^*} \epsilon + \frac{1}{2} B_c^* \eta^2.$$

which then becomes

$$\eta \approx \sqrt{\frac{2\alpha_c^*}{2B_c^{*2}} \epsilon}. \tag{B15}$$

Finally, this means that $\alpha - \alpha_c^* \underset{B \to B_c^*}{\sim} (B - B_c^*)^{1/2}$.

2.   Case II: $B < B_c^*$, travelling front solution

In addition to the previous case, there can also be a travelling front solution, for which we assume the asymptotic form $\psi(\xi) \equiv \psi_{t\to\infty}(\xi) \sim \exp(-\alpha\xi)$ for large $\xi \equiv \tau - vt$. This assumption reduces Eq. (A9) to

$$-\alpha \exp(\alpha v) + \exp(\alpha v) = K \exp(-\alpha B), \tag{B16}$$

and then Eq. (B16) can be written as

$$\frac{1-\alpha}{K} \exp(\alpha v) = \exp(-B\alpha). \tag{B17}$$

The two types of asymptotic forms, together with the exponential decay assumption of ψ can be consistent with each other if $v = 0$ when $B > B_c^*$.

Case $B < B_c^*$:

For $B < B_c^*$, we assume that for large ξ, $\psi(\xi) \sim \exp(-\alpha_c^*\xi)$, leading to

$$\frac{1-\alpha_c^*}{K} \exp(\alpha_c^* v) = \exp(-B\alpha_c^*). \tag{B18}$$

Since $\tilde{\alpha}_c$ is related to B_c^* through Eq. (B12), combining with (B18) leads to $v = B_c^* - B$.

We close SI B with the note that Eq. (B3) we have analytically solved for $K = 2, 3, 4$ and 5, and note that the solutions become progressively complex with increasing values of K.

SI C: Real-world data statistics

The data sets for the high school and the workplace were taken from `sociopatterns.org` [26, 27]. In these datasets, agents — pupils and employees respectively — were tracked by wearable sensors, and contacts among agents were recorded at 20 second intervals (the time interval between two consecutive time steps is therefore 20 seconds). The time series of the agents' contacts at discrete time steps yielded the corresponding temporal networks, which provided us with the temporal adjacency matrix $\mathbf{A}(t)$.

As described in the main text below Fig. 7, we constructed the "event representations" of these temporal networks, with each disjoint network component at every time step defining an event. Because of the ways the sensors work, an (example) event of agents a_1, a_2 and a_3 at some time step may be registered as simultaneous contacts between a_1 and a_2, and between a_1 and a_3, while a contact between a_2 and a_3 is not registered. In order to suit the current purpose however, in the event representation we consider it as an event where all three agents are simultaneously in contact with each other.

The statistics for the data sets that were used in Fig. shown in Table II. [Sparsity in Table II is defined as the percentage of agents that participated in single-agent events, summed over all temporal layers. For example, in Fig. 7(b), the sparsity is obtained as $(0 + \frac{1}{2} + \frac{1}{2})/3 = 1/3 \approx 33.33\%$.]

Quantity	Highschool data	Workplace data
Total time steps	8937	9679
Unique agents	328	208
Events	131251	33572
Events per timestep	14.68 ± 4.30	3.47 ± 2.13
Agents per event	11.70 ± 12.59	2.45 ± 0.72
Sparsity	47.63%	95.90%

TABLE II. Summary statistics of the temporal network data sets from a highschool [26] and a workplace [27].

SI D: Effects of heterogeneity and sparsity of STNs on criticality

In order to get an insight into what causes higher-order transitions for real-world temporal networks in contrast to second order transitions for the MF or STN cases [as in Fig. 2(a)], we simulated delay developments on STNs upon introducing sparsity and heterogeneity into them.
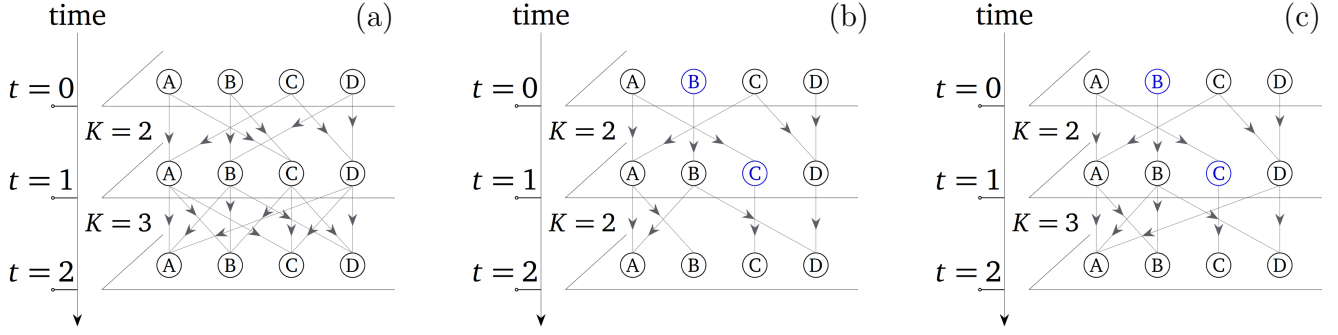
FIG. 9. Schematics for synthetic temporal networks (STNs) with heterogeneity and sparsity. (a) With heterogeneity, but no sparsity: K is the same for all system components per time step, but is different across time steps (for example, $K = 1$ and 3 at $t = 0$ and 1 respectively. (b) With sparsity, but no heterogeneity. Sparse nodes (blue) are created by connecting the system components only to itself between time steps t and $t+1$. (c) A temporal network with both heterogeneity and sparsity, as seen in real-world temporal networks.

We define heterogeneity in STNs as the value of K being different at different time steps — albeit the same for all firms at any given time step [a heterogeneous, but not sparse STN is shown in Fig. 9(a)]. Sparsity in a STN is defined in line with SI C: it is determined by the average percentage of system components whose delay at any given time step does not influence any other ones in the following time step [a sparse STN without heterogeneity is shown in Fig. 9(b), the sparsity of this network is $\left(\frac{1}{4} + \frac{1}{4} + 0\right)/3 = 1/6 \approx 16.67\%$]. Defining them in this way means that we can separately control heterogeneity and sparsity [and if needed, can also combine them, as shown in Fig. 9(c)] while synthesizing temporal networks.
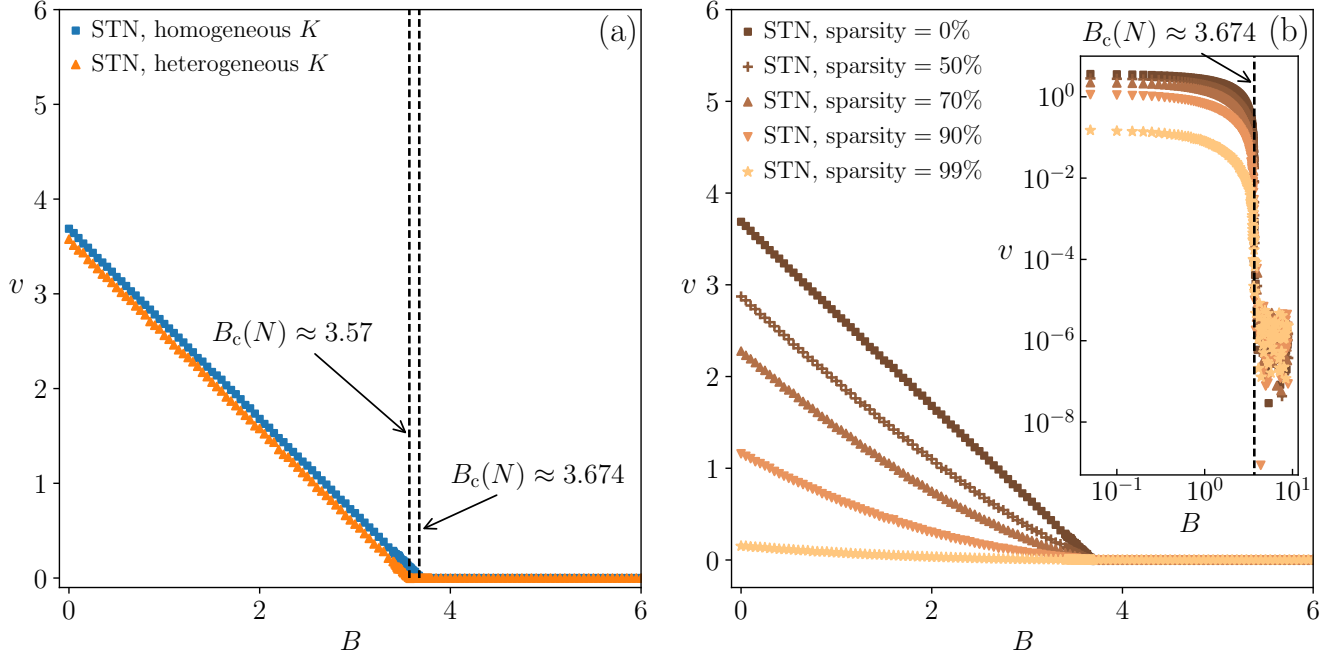

FIG. 10. Effect of heterogeneity alone (a) and sparsity alone (b) on criticality for $N = 10,000$. In panel (a) the order parameter for homogeneous STN with $K = 5$ is plotted alongside the one for a heterogeneous STN with $K \sim \text{Uniform}\{2, 3, \ldots, 8\}$. Heterogeneity alone changes the magnitude of $B_c(N)$, but does not change the order of transition. In contrast, panel (b) shows that sparsity alone does not change the magnitude of $B_c(N)$, but pushes the transition to be of higher order. See text for details.

The results of our experiments with delay developments on (a) heterogeneous but not sparse and (b) sparse but homogeneous temporal networks for $N = 10,000$ are shown in Fig. 10(a) and (b) respectively. In panel (a) the value of K per time step is chosen from a uniform distribution between 1 and 9; we choose this range in order to maintain

the average K at 5, allowing us a comparison to Fig. 9(a) for which $K = 5$. Evidently, the transition is still second order, but heterogeneity alone in K lowers the value of $B_c(N)$ [c.f. 10(a)]. In contrast, sparsity alone does not change the magnitude of $B_c(N)$ but pushes the order of transition to be of higher order.

SI E: Finite temperatures, continuous tree

The aim of this section is to (a) make a more direct connection with the Directed Polymer problem and provide a generalisation of our model to non-zero temperatures that reveals a full line of transition in the plane (buffer amplitude, temperature) – see Fig. 11; and (b) give another exact calculation of the properties of the model on continuous tree-like structures, rather than in the mean-field limit considered in the main text. Reassuringly, the results obtained on trees are very similar to those obtained in the mean-field limit.

Finite temperature generalisation

To make apparent the connection with the directed polymer (DP) problem, it is interesting to define a "finite temperature" extension of our model. Introducing the variable $Z_i(t) = e^{\beta \tau_i(t)}$, where β is the inverse temperature parameter, the recursion is generalized as

$$Z_i(t+1) = e^{\beta \epsilon_i(t)} \left(1 + e^{-\beta B} \sum_{j \in \partial_i} Z_j(t) \right) \tag{E1}$$

where ∂_i denote the set of K sites connected to i. When $\beta \to +\infty$ one recovers the "zero temperature" recursion considered in the main text:

$$\tau_i(t+1) = \epsilon_i(t) + \max \left(0, \max_{j \in \partial_i} (\tau_j(t) - B) \right) \tag{E2}$$

The variable $Z_i(t)$ can be interpreted as a canonical partition function for polymers ending at i, t and the variable $\tau_i(t) = \log Z_i(t)$ as minus the free energy. Note that at finite temperature the variable $\tau_i(t)$ can become negative.

Cayley tree

We now study the model on the Cayley tree (CT) where each site at generation $t+1$ is connected to K sites at generation t. Since the $\epsilon_i(t)$ are i.i.d., assuming that the leaves at $t = 0$ to be identical and independent, those at generation t are also i.i.d. and one can rewrite (E1) as a recursion for a single random variable $Z(t)$

$$Z(t+1) = e^{\beta \epsilon(t)} \left(1 + e^{-\beta B} \sum_{j=1}^{K} Z^{(j)}(t) \right) \tag{E3}$$

where $Z^{(j)}(t)$ are K independent copies of the random variable $Z(t)$. This is a variant of the DPCT problem studied in [24]. Let us introduce, as in that work, the generating function, defined for $\tau \in \mathbb{R}$

$$G_t(\tau) = \langle e^{-e^{-\beta \tau} Z(t)} \rangle \tag{E4}$$

with $G_t(\tau) \in [0,1]$, $G_t(-\infty) = 0$ and $G_t(+\infty) = 1$. From (E3), and since the $Z^{(j)}(t)$ for different j are independent, one immediately obtains the recursion

$$G_{t+1}(\tau) = \int_0^{+\infty} d\epsilon \, p(\epsilon) e^{-e^{-\beta(\tau-\epsilon)}} [G_t(\tau + B - \epsilon)]^K \tag{E5}$$

where we denote $p(\epsilon)$ the PDF of $\epsilon(t)$. Since $G_t(\tau) = \langle e^{-e^{-\beta(\tau-\tau(t))}} \rangle$ one has

$$\lim_{\beta \to +\infty} G_t(\tau) = \langle \theta(\tau - \tau(t)) \rangle = \text{Prob}(\tau(t) < y) = P_t^<(\tau) = \int_0^\tau d\tau' \, P_t(\tau') = 1 - \Psi_t(\tau) \tag{E6}$$

Hence in the limit $\beta \to +\infty$ the recursion (E5) becomes

$$P_{t+1}^<(\tau) = \int_0^\tau d\epsilon \, p(\epsilon)[P_t^<(\tau + B - \epsilon)]^K \tag{E7}$$

This relation is the primitive of the one in (3) which can be recovered by taking a derivative of (E7) w.r.t. τ and using $\frac{d}{d\tau}P_t^<(\tau) = P_t(\tau) = \psi_t(\tau)$. So we have checked that (3) is exact on the Cayley tree.

Continuous tree

As in [24] it is easier to study the continuum version of the tree. So now t is a continuum variable and the tree branches in two with a rate φdt. We assume that the noise becomes Brownian in the limit, with a drift $\bar{\epsilon}$ (corresponding to the average delay for individual events in the discrete case)

$$\epsilon(t) \to \bar{\epsilon} dt + \sigma dW(t) \tag{E8}$$

where $W(t)$ is a standard Brownian motion. Now $Z(t)$ becomes a continuous process in time and its evolution on a time interval dt is as follows

$$Z(t + dt) = \begin{cases} Z(t)e^{\beta(\bar{\epsilon} dt + \sigma dW(t))} & \text{with prob.} \quad 1 - \varphi \, dt \\ 1 + e^{-\beta B}\sum_{j=1}^K Z^{(j)}(t) & \text{with prob.} \quad \varphi \, dt \end{cases} \tag{E9}$$

With the same definition of the generating function $G_t(\tau)$ as in (E4) and using Ito's rule we find that under the evolution (E9) it satisfies the partial differential equation

$$\partial_t G_t(\tau) = -\bar{\epsilon}\partial_\tau G_t(\tau) + \frac{\sigma^2}{2}\partial_\tau^2 G_t(\tau) + \varphi(e^{-e^{-\beta\tau}}G_t(\tau + B)^K - G_t(\tau)) \tag{E10}$$

which is the continuum analog of (E5) (with the same boundary conditions).

Moving phases: high and low temperature phases. Let us look for a traveling wave solution. We insert

$$G_t(\tau) = w(\tau - vt) \quad , \quad w(-\infty) = 0 \quad , \quad w(+\infty) = 1 \tag{E11}$$

One sees that if $v > 0$ the term $e^{-e^{-\beta\tau}} \approx e^{-e^{-\beta vt}} \approx 1$ in the region of the front hence one obtains

$$\frac{\sigma^2}{2}w''(y) + (v - \bar{\epsilon})w'(y) + \varphi(w(y + B)^K - w(y)) = 0 \tag{E12}$$

Proceeding as in [24] we look for a tail at large $y > 0$

$$w(y) \approx 1 - e^{-Ay}. \tag{E13}$$

Collecting the terms proportional to e^{-Ay} one obtains the condition which determines the velocity as a function of A

$$v = \mathsf{v}(A) := \bar{\epsilon} + \frac{\varphi(Ke^{-AB} - 1)}{A} + \frac{\sigma^2}{2}A \tag{E14}$$

It remains to determine A. We will proceed as in [24]. First one notes from (E4) that for large positive τ, $G_t(\tau) \approx 1 - e^{-\beta\tau}\langle Z(t)\rangle$. On the other hand one easily finds from the recursion (E9), or equivalently from (E10), that $\langle Z(t)\rangle \approx e^{\beta v(\beta)t}$ (which is exact for any β, where the function $\mathsf{v}(A)$ is defined in (E14)). When this "first moment tail" is also in the front region defines the *high temperature phase*. In this phase $A = \beta$ (i.e. from the boundary condition at $y = +\infty$) and $v = \mathsf{v}(\beta)$.

On the other hand the function (A) defined in (E14) has (for $K > 1$) a unique minimum as a function of A, which we denote $A = A_c$. As β increases from zero, the front velocity $v = \mathsf{v}(\beta)$ decreases in the high temperature phase and eventually reaches its minimum value. As in [24] one obtains that it *freezes* at the temperature $\beta_c = A_c$ hence

$$v = v_c = \mathsf{v}(A_c) \quad , \quad \beta > \beta_c = A_c \tag{E15}$$

which defines the low temperature (glass) phase. In that phase $1 - G_t(\tau) \approx \tau e^{-\beta_c \tau}$ at large τ (a much slower decay than the one in the first moment tail, which is now valid only in the far forward region of the front). The value of $\beta_c = A_c$ is determined by the root of

$$(1 + A_c B)e^{-A_c B} = \frac{1}{K} + \frac{\sigma^2}{2K\varphi}A_c^2 \tag{E16}$$

The r.h.s is an increasing function of A_c starting from $1/K$ for $A_c = 0$, whereas the l.h.s. is a decreasing function of A_c (one has $(1 + x)e^{-x} = 1 - \frac{x^2}{2} + O(x^3)$ at small x), hence there is a unique root. The corresponding value of the velocity in the low temperature phase is

$$v_c = \bar{\epsilon} + \frac{\sigma^2}{2}A_c + \frac{\varphi(Ke^{-A_c B} - 1)}{A_c} \tag{E17}$$

Note that for $B = 0$ (in the absence of buffers) one has

$$\mathsf{v}(A) := \bar{\epsilon} + \frac{\varphi(K - 1)}{A} + \frac{\sigma^2}{2}A \quad , \quad \beta_c = A_c = \sqrt{\frac{2\varphi}{\sigma^2}(K - 1)} \quad , \quad v_c = \bar{\epsilon} + 2\sqrt{\frac{\varphi\sigma^2}{2}(K - 1)}. \tag{E18}$$
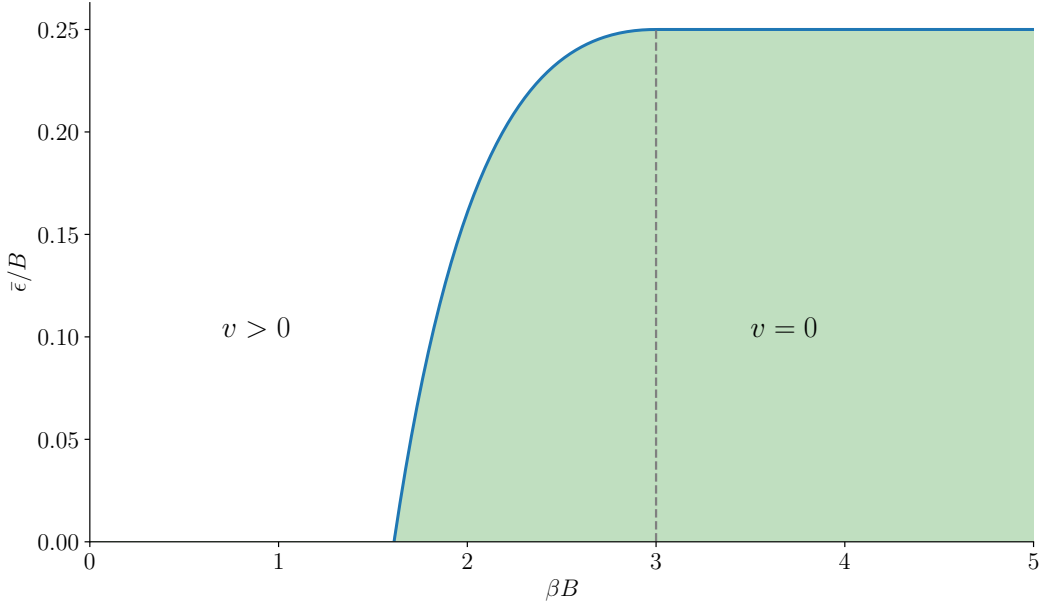

FIG. 11. Phase diagram of the model in the plane (inverse temperature βB, inverse buffer strength $\bar{\epsilon}/B$), in the limit where B and $\bar{\epsilon}$ are both large, and $\varphi = 1$. Note that for low enough temperature, i.e. for $\beta > \beta_c = r_c/B$, the critical buffer strength B_c^* is independent of temperature. For $\beta < \beta_c = r_c/B$, on the other hand, the critical buffer size is temperature dependent. For $\beta B < \log K$ only the "depinned" phase $v > 0$ exists for $\bar{\epsilon} > 0$. Here we have chosen $K = 5$ for which $r_c \approx 3$ and $\log K \approx 1.61$.

Pinned phase. The above analysis is correct only whenever the front velocity $v > 0$. When the velocities determined above, i.e. $v = \mathsf{v}(\beta)$ for $\beta < \beta_c$ and $v = v_c$ for $\beta > \beta_c$, vanish then one enters the "pinned" phase where $G_t(\tau)$ reaches a stationary limit $G_\infty(\tau)$ for $t \to +\infty$. This corresponds to the situation where delay do not accumulate and requires that B increases beyond a threshold value B_c^*, which however has a different expression depending on whether $\beta < \beta_c$ and $\beta > \beta_c$. Hence there are now two phase boundaries to the pinned phase.

The expression of the phase transition boundary considerably simplifies in the limit $\bar{\epsilon} \to \infty$, $B \to \infty$ and $\beta \to 0$ with $\bar{\epsilon}/B$ and βB remaining $O(1)$. In that limit the terms containing the noise amplitude σ become subdominant. We then get that $A_c B = r_c$ with r_c given by the solution of

$$(1 + r_c)e^{-r_c} = \frac{1}{K}$$

For $K = 5$, for example, the numerical value of r_c is very close to 3. The phase boundary can the be computed to be:

$$\begin{cases} \frac{\bar{\epsilon}}{B} &= \frac{\varphi}{1+r_c} \qquad (r \geq r_c) \\ \frac{\bar{\epsilon}}{B} &= \frac{\varphi}{r}(1 - Ke^{-r})^+ = \frac{\varphi}{r}\left[1 - K^{1-r/r_c}(1+r_c)^{-r/r_c}\right]^+ \qquad (r \leq r_c) \end{cases}$$

where $r := \beta B$. Here we restrict to $\bar{\epsilon} > 0$, in the spirit of the model in the main text. The corresponding phase diagram in the plane $r, \bar{\epsilon}/B$ is given in Fig. 11. One sees that the zero temperature phase transition found in the main text survives at non zero temperatures, but disappears at high temperatures where only the "depinned" phase $v > 0$ exists.

The phase diagram looks qualitatively similar values of B and $\bar{\epsilon}$ that are not infinitely large. Also, one can check that the behaviour of v when B is close to B_c^* (when it exists) is always linear, i.e. $v \propto B_c^* - B$.